# *TCR binding to a peptide-MHC complex raises a drawbridge for CD3 cross-membrane signaling*

Floris J. van Eerden[a*], Aalaa Alrahman Sherif[b], Mara Anais Llamas-Covarrubias[b] & Daron M. Standley[b*]

[a]Immunology Frontier Research Center, Osaka University, 3-1 Yamadaoka, Suita, Japan
[b]Research Institute for Microbial Diseases, Osaka University, 3-1 Yamadaoka, Suita, Japan

[*]Corresponding author

E-mail: Floris van Eerden fvaneerden@ifrec.osaka-u.ac.jp
Daron Standely standley@biken.osaka-u.ac.jp

# Abstract

The mechanism of T cell triggering upon engagement with a peptide-MHC (pMHC) complex remains a challenging problem. In order to observe structural and dynamics changes in the T cell receptor (TCR) upon pMHC binding, we carried out coarse grained molecular dynamics simulations of TCR-only and TCR-pMHC systems starting from a recently solved cryo-EM structure of the TCR and CD3 co-receptors. The simulations were performed in biological membranes for an aggregated length of 2 ms. We observed that, while unengaged TCRs adopted conformations that bent and restricted the dynamics of the CD3 co-receptors, the pMHC-bound TCRs adopted elongated conformations that allowed CD3 co-receptors to diffuse more freely. In this way, the TCR-pMHC pair acted as a "drawbridge", licensing the dynamics of the CD3 co-receptors, resulting in signal transmission across the plasma membrane.

# Introduction

T cell receptors (TCRs) play a central role in adaptive immunity by recognizing peptide antigens presented by major histocompatibility complex (MHC) molecules. The binding of agonistic, but not antagonistic, peptide-MHC (pMHC) complexes results in TCR triggering, a set of biochemical changes in the cytoplasmic regions of the CD3 complex (van der Merwe and Dushek, 2011) that can subsequently lead to T cell activation. The effector functions of activated T cells range from the killing of infected cells, to inhibition of immune responses, to

establishment of memory of specific peptide antigens. In line with their importance, TCRs have been intensively studied over the last several decades; however, the mechanisms linking pMHC engagement with TCR triggering remain elusive.

In the last decade, a number of models of T cell activation and TCR triggering have been proposed, each emphasizing different aspects of the phenomena. The relationship between initial pMHC engagement and cytoplasmic signaling is treated by the *mechanosensor model*. In this model, TCRs discriminate agonistic from antagonistic pMHCs via catch bond formation (Sokurenko et al., 2008) (Zhu et al., 2019) (Feng et al., 2018; Hwang et al., 2020), which transfers force from the pMHC-TCR interface to the TCR-CD3 interface via the FG loop on the TCR (Das et al., 2015; Kim et al., 2009). Alternatively, the *kinetic proofreading* model emphasizes that pMHC-TCR complex lifetimes, rather than forces per se, are critical for distinguishing agnostic from antagonistic pMHCs (Lo et al., 2019). The *TCR bending mechanosignal model* argues that TCR-pMHC engagement results in changes in membrane curvature that promote conformational changes in the receptors that are transmitted to the cytoplasmic side (Al-Aghbar et al., 2022). Finally, in the *allosteric relaxation* model TCR-pMHC binding results in decoupling of interactions between TCR and CD3ζ (Rangarajan et al., 2018; Brazin et al., 2018; Lanz et al., 2021). While the models differ in detail, each requires a yet to be defined mechanical communication between the TCR and the CD3 co-receptors that is transmitted through the membrane. The TCR-CD3 linkage is crucial, since CD3s, but not TCRs, contain cytoplasmic immunoreceptor tyrosine-based activation motifs (ITAMs), which become phosphorylated upon activation.

On the cytoplasmic side, the *ITAM sequestration model* argues that the CD3 ITAMs are buried in the membrane in the resting state but, upon the proper extracellular signal, become exposed to the cytoplasmic lymphocyte-specific protein tyrosine kinase (Lck), whereupon a downstream signaling cascade occurs (Xu et al., 2008; Aivazian and Stern, 2000). Other models, including *kinetic segregation* (Nika et al., 2010; Davis and van der Merwe, 2006) and *aggregation* (Saito and Yokosuka, 2006; Cai et al., 2018) emphasize morphological changes in the synapse that forms between the engaged T cell and APC. Other studies have reported that individual TCRs can become triggered (Brameshuber et al., 2018), suggesting that there is merit in learning from simple TCR-pMHC systems.

In 2019, the first full-length structure of a TCR with CD3 co-receptors was determined by single particle cryo-EM (Dong et al., 2019). Interestingly, this structure revealed that the extracellular domain (EC) of the TCR is bent 144° with respect to the membrane normal. This observation raised the question of whether the angle between the TCR EC and transmembrane domain (TM) is dynamic. Molecular dynamics studies based on the complete TCR structure in a membrane demonstrated that the TCR is indeed flexible and that the TCR headgroup can adopt a range of different conformations (Prakaash et al., 2021; Pandey et al., 2021).

These recent findings raise new questions. Of particular interest is how pMHC engagement affects the dynamics of the TCR. Such dynamics may shed much needed light on the nature of the communication between the TCR and CD3 co-receptors in T cell triggering. To this end, we carried out extended molecular dynamics simulations of two systems: a "TCR-only" system (Figure 1A), which consisted of only the TCR CD3 co-receptor complex embedded in a membrane, and a "TCR-pMHC" system, consisting of two opposing membranes: one containing a pMHC and the other containing a TCR CD3 co-receptor complex (Figure 1B). The cumulative simulation time for each system was 1 ms. Although there have been previous studies of a TCR in complex with a pMHC (Wan et al., 2008; Bello and Correa-Basurto, 2016; Alba et al., 2020), to our knowledge, this is the first attempt to compare free and pMHC-engaged TCRs based on the complete cyro-EM structure (Dong et al., 2019), which critically contains the CD3 co-receptors.

Consistent with earlier work, we observed a wide range of conformational states for the TCR-only system. As might be expected, the TCR-pMHC system was more restricted. However, what was surprising is that pMHC engagement was associated with significantly larger dynamic motions in the CD3 coreceptors. In our simulations, TCR-pMHC engagement allowed the CD3 co-receptors to move around the TCR. Importantly, these simulations did not contradict key evidence of previously-proposed triggering models. For example, in agreement with the mechanosensor and kinetic proofreading models, we observed a critical role of the FG loop on CD3 dynamics. Our simulations also recapitulated key findings of the allosteric relaxation model. Taken together, our findings show that dynamics is critical to understand the communication between the extracellular and cytoplasmic events that occur in TCR triggering.

# Results

*Description of the simulation systems*

To study the dynamics of the TCR under resting and pMHC-engaged conditions, two systems were constructed: A TCR-only system, in which a single TCR was embedded in a POPC bilayer (Figure 1A) and a TCR-pMHC system (Figure 1B). The later system was composed of two opposing POPC bilayer slabs; the lower representing the T cell membrane and containing a TCR, and the upper representing the APC membrane in which a pMHC was embedded. The TCR in the simulations was a fusion between the complete TCR cryo-EM structure (PDB ID 6jxr) and a crystal structure of a pMHC-bound TCR (PDB ID 3qiu), which lacked the TCR TM (Dong et al., 2019) (Newell et al., 2011). Harmonic potentials based on the crystal structure were used to bind the TCR to the pMHC; the potentials were applied in a stepwise manner during 1.5 µs preparatory simulations to let the system slowly adjust (Figure S1). A pore was created in the APC membrane in order to allow the flow of solvent between the two membrane compartments, which was required in order for the distance between the APC and T cell membranes to change

naturally. For each system, one hundred 10 µs production runs were performed, totaling 1 ms per system.

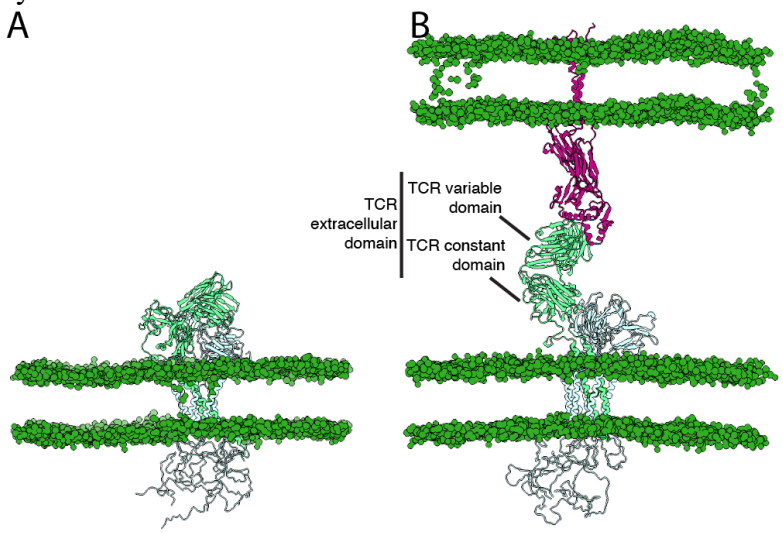


**Figure 1: The TCR only and TCR-pMHC simulations systems.** Snapshots of the TCR-only (A) and TCR-pMHC (B) simulation systems. The TCR is in lime, CD3 co-receptors in cyan, pMHC in purple and lipid headgroups in green. Note that in the TCR-pMHC channel a pore is present in the upper membrane to allow the flow of solvent between the two compartments, which is why headgroup beads are visible in the membrane interior. Solvent and lipid tails are not shown for clarity. In panel B the TCR variable (V) and TCR constant (C) domains are indicated. The TCR extracellular domain (EC) encompasses the variable and constant domains.

*CD3 epsilon chains exhibited a wider range of motion upon TCR-pMHC engagement.*
Iso-occupancy surfaces were calculated to study the distribution on the CD3 epsilon chains in the simulations. The CD3 epsilon chains in the TCR-pMHC simulations sampled a larger area around the TCR compared to the TCR-only simulations (Figure 2). The iso-occupancy surface of the CD3 epsilon chains in the TCR-only simulations had a clear minimum close to the position of the CD3ζ chains (Figure 2A), in contrast the CD3 epsilon chains in the TCR-pMHC simulations sampled the region around the TCR completely (Figure 2B). Interestingly the TCR-only iso-occupancy surface was not symmetric, with the occupancy being especially low around the CD3ζ chain that is next to CD3γ (hereafter CD3$\zeta^{\gamma}$).

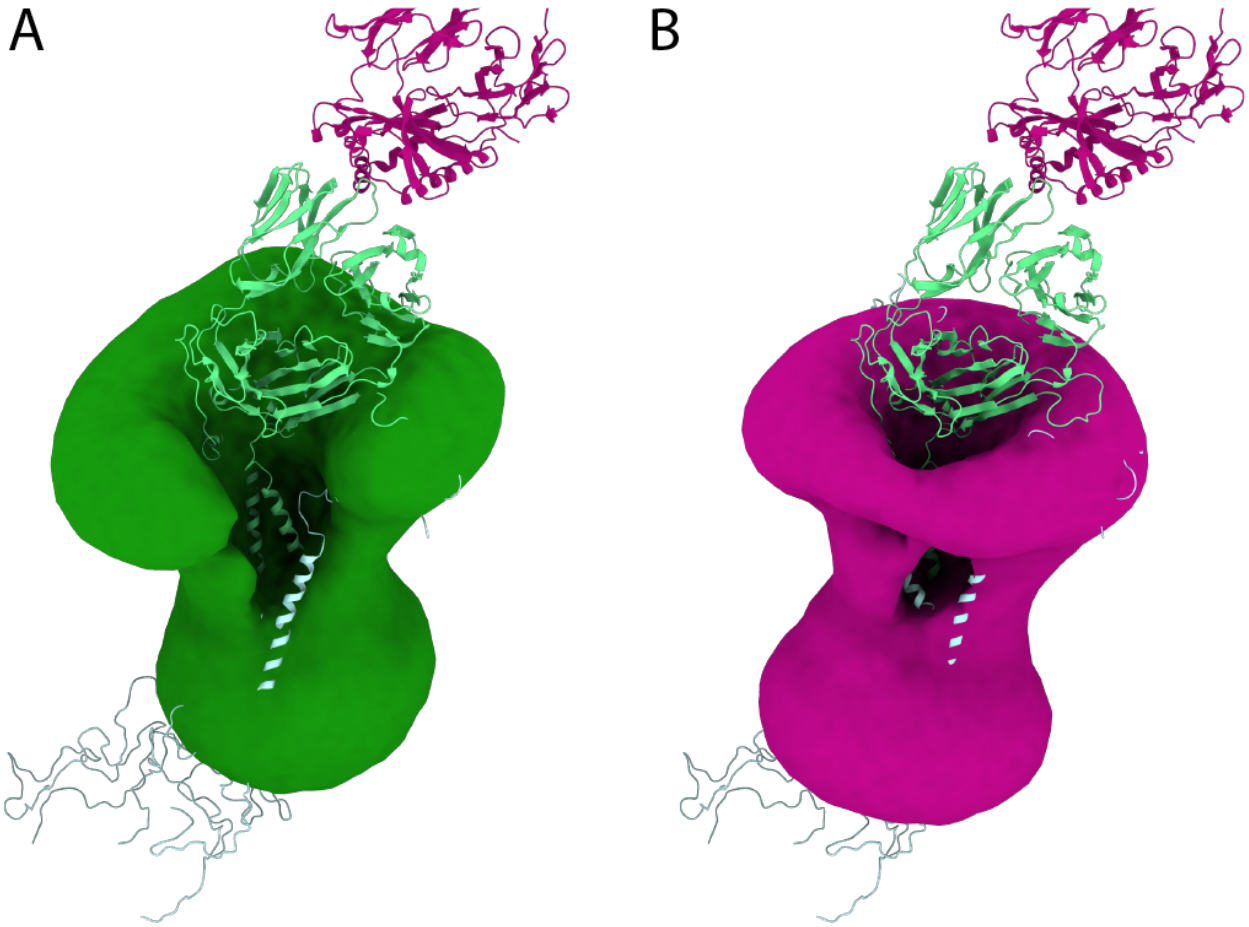


**Figure 2: Iso-occupancies of CD3$\varepsilon^{\gamma}\varepsilon^{\delta}$ around the TCR αβ chains**. Iso-occupancy of CD3$\varepsilon^{\gamma}\varepsilon^{\delta}$ in the TCR-only simulation is shown in green (panel A), and in purple for the TCR-pMHC simulation (panel B). The TCR is colored in lime, CD3 co-receptors in cyan (mostly obscured by the iso-surfaces) and pMHC in purple.

*pMHC engagement resulted in fewer contacts between the CD3 co-receptors and the TCR variable domain*

To get a better understanding of the reasons for the difference in CD3 co-receptor distribution in the simulations systems, the contacts between the CD3 co-receptors and the TCR chains were analyzed. There were clear differences in the quantity and type of contacts between the TCR and the CD3 co-receptors in the TCR-only and TCR-pMHC simulations, especially for contacts involving the TCR variable domain (V) (Figure 3 and Figure S2). The epsilon chain in contact with CD3γ (hereafter CD3$\varepsilon^{\gamma}$) (Figure 3A) and the CD3γ chain (Figure 3B) were consistently in contact with the TCR V in the TCR-only simulations; however, these interactions virtually disappeared in the TCR-pMHC simulations.

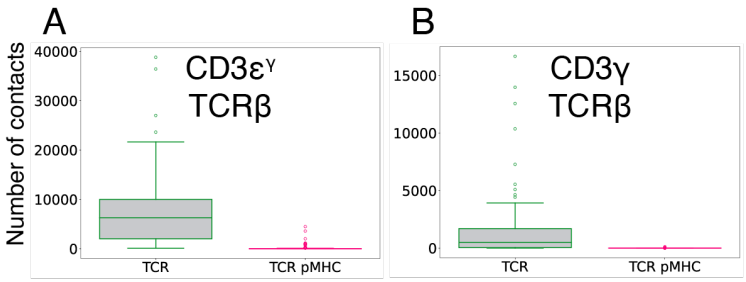


**Figure 3: TCR CD3 co-receptor contacts.** The number of contacts between the TCRβ variable domain and the indicated CD3 chains in the TCR-only (green box plots) and TCR-pMHC (pink box plots). Note that the y-axis varies between the three plots. Please refer to Figure S2 for the contacts specified per residue.

*TCR straightens upon pMHC engagement*

The TCR adapted qualitatively different conformations upon pMHC binding, as measured by the angle between the TCRβ transmembrane domain (TM) and extracellular domain (EC) (Figure 4). In the TCR-only system, in which the TCR EC folded over the CD3 co-receptors (Figure 1A), the TCR adopted predominantly bent conformations (smaller angles), with a peak in the distribution at 104°. Such bending was observed in previous simulations of the same starting structure (Pandey et al., 2021). In contrast, the TCRs in the TCR-pMHC system, for which the many interactions with CD3 were broken, tended to adopt an extended and open conformation (larger angles, with the peak of the distribution at 150°) where the TCR EC tilted away from the CD3 EC domains (Figure 4 and Figure 1B). The TCR-pMHC simulations also sampled a narrower distribution of angles, with a full-width at half-maximum (FWHM) of approximately 30°, than the TCR-only simulation (FWHM 40°).

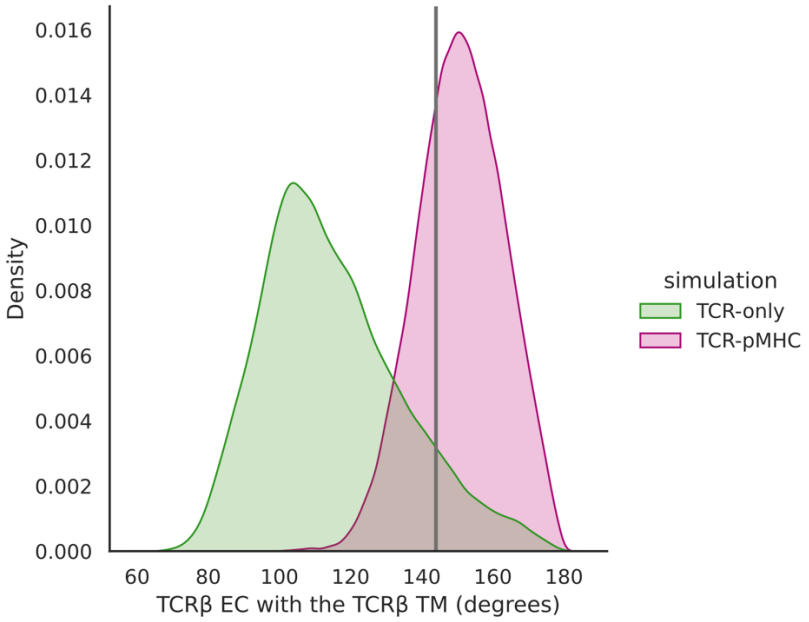


**Figure 4: Angle distributions of the TCRβ EC with the TCRβ TM.** Angle distribution of the TCR-only (lime) and TCR-pMHC (pink) systems. The angle of the cryo-EM structure (vertical line) was 144°.

*TCR acts as drawbridge*

When combining these three observations, a mechanism emerges in which the TCR adopts a bent conformation in the "TCR-only" simulations, with the TCR V binding to the CD3 co-receptors, thereby hindering their movement. Upon pMHC binding, the TCR adopts a more extended conformation, which breaks the bonds between the TCR V region and the CD3 co-receptors, subsequently allowing them to diffuse around the TCR. The TCR thus acts as a "drawbridge", in which the opening of the bridge (pMHC binding) allows the passing of the co-receptors, leading to increased dynamics across the membrane (Figure 5). We hypothesize, over time, such unrestricted dynamics results in rearrangements of the ITAMS, ultimately resulting in their phosphorylation.

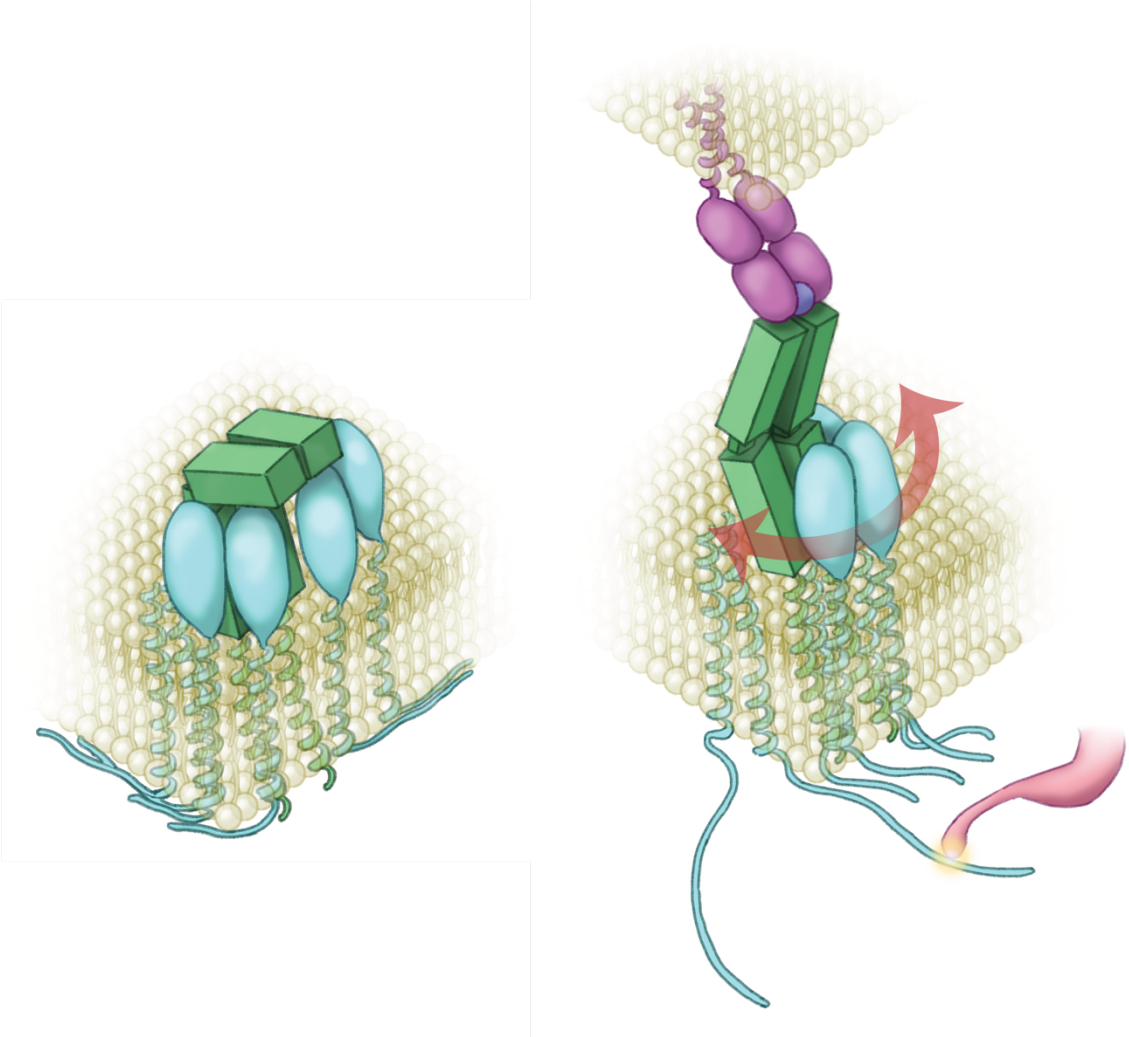

**Figure 5 TCR-pMHC binding acts as a drawbridge for the CD3 co-receptors.** In the left panel the unengaged TCR is bent over the CD3 co-receptors, preventing their diffusion. Upon pMHC binding (right panel), the TCR straightens, resulting in release of the CD3 co-receptors, allowing their diffusion around the TCR. This freedom facilitates exposure of cytoplasmic tails from the membrane, licensing phosphorylation of the ITAMs.

*Role of the TCRβ FG loop*

Long range perturbations were observed in previous experimental studies of the TCR upon pMHC binding, notably in three key regions: the TCRα AB loop; the TCRβ H3 helix; and the TCRβ FG loop (Mariuzza et al., 2020; Natarajan et al., 2017; Rangarajan et al., 2018). In agreement with these experimental observations, differences in these regions upon pMHC binding were observed in our simulations as well. Both the TCRα AB loop and the TCRβ H3 helix exhibited increased interactions with one of the CD3 epsilons upon pMHC binding. The TCRα AB loop contacted the CD3 epsilon of the CD3εγ dimer (hereafter CD3$\varepsilon^{\gamma}$) predominantly in the TCR-pMHC simulations (Figure 6A), while the TCRβ H3 helix made more contacts with the CD3 epsilon of the CD3εδ dimer (hereafter CD3$\varepsilon^{\delta}$) in the TCR-pMHC simulation (Figure

6B). The TCRα AB loop and the TCRβ H3 helix are located out of reach from CD3$\varepsilon^{\gamma}$ and CD3$\varepsilon^{\delta}$, respectively, in the cryo-EM structure; this made interactions between these regions unlikely to occur in the TCR-only systems, in which the CD3 co-receptor movement is restricted. Upon pMHC binding, however, the interactions between the TCR EC and the CD3 co-receptors, were broken, resulting in increased movement of the CD3 epsilon chains which could subsequently interact with previously inaccessible areas of the TCR.

Experiments and simulations suggested that the TCRβ FG loop has an important role in TCR triggering and that the TCR FG loop dynamics changes upon pMHC binding (Kim et al., 2009; Das et al., 2015; Rangarajan et al., 2018). We observed that the TCRβ FG loop contacted CD3$\varepsilon^{\gamma}$ in the TCR-only simulations more than in the TCR-pMHC simulations (Figure 6C). Inspection of the trajectory showed that the TCRβ FG loop blocked the diffusion of the CD3εγ dimer proximate to TCRβ. In the pMHC simulations, the TCRβ FG loop moved up and allowed diffusion of the CD3εγ.

These data suggest that the TCRβ FG acts as a break on the system, preventing the diffusion of the CD3εγ dimer when the TCR is unbound. This also explains the asymmetry observed in the CD3 epsilon distributions in the TCR-only simulations (Figure 2A). The iso-occupancy maps in the TCR-only simulation lack density specifically around CD3$\zeta^{\gamma}$, while there is clear density around the CD3ζ chain that is next to CD3$\varepsilon^{\delta}$ (hereafter CD3$\zeta^{\varepsilon}$). While the positioning of the CD3 co-receptors around the TCR is fairly symmetric, the TCRα chain lacks the equivalent of the TCRβ FG loop. This grants CD3εδ the possibility to occasionally move alongside the TCRα chain, while an equivalent movement by CD3εγ is blocked by the TCRβ FG loop. This also can be seen the contacts between TCRα and the CD3 epsilon chains (Figure S3) where the difference between the TCR-only and TCR-pMHC simulations is much smaller compared to the difference in contacts between TCRβ and CD3εγ (Figure 3). Consistently, a reduction in TCR CD3ζ interactions has been observed upon pMHC binding in DDM stability assays (Lanz et al., 2021). In line with this evidence, we observed a reduction in the contacts between the CD3ζ chains and TCRβ upon pMHC binding (Figure S4).

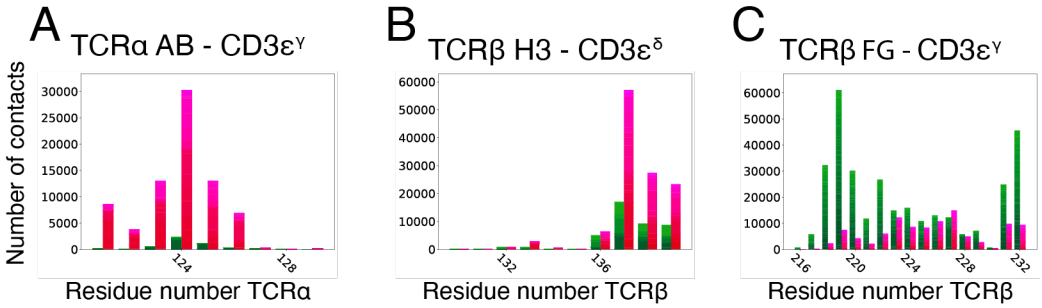


**Figure 6: Cumulative TCR – CD3 contacts.** Contacts between CD3 co-receptors and the TCRα AB loop (A), TCRβ H3 helix (B) and the TCRβ FG loop (C) in the in TCR-only (green bars) and TCR-pMHC simulations (red bars). Contacts are summed over all simulations and are shown as gradients, where each step in the gradient represent the contacts in a single simulation. Residue numbers of the TCRα or TCRβ chains are shown on the x-axis. Note that the y-axis varies between the plots.

# Discussion

The critical role of T cells in host immunity has inspired decades of research into TCR structure and function. In spite of this vast volume of work, the molecular mechanism of TCR-mediated signal transduction from the pMHC to the CD3 ITAMs remains an open question. Even if we take for granted that agnostic pMHC complexes induce sufficient force or persist for a requisite threshold of time, a complete understanding of TCR triggering must also include some form of coupling between the TCR and the CD3 co-receptors. Without this coupling, the causes of triggering events in the cytoplasm remain a mystery.

It has been proposed that catch bonds effect the dynamics of the TCR and, by extension, the TCR-CD3 interface. Recent NMR studies (Rangarajan et al., 2018; Natarajan et al., 2017) support this line of reasoning. Specifically, three regions (TCRβ FG, TCRα AB, and TCRβ H3) have been shown to exhibit chemical shift signal perturbations upon pMHC binding, implying that pMHC-TCR interactions mediate long-range changes in TCR structure, dynamics, or both (Beddoe et al., 2009). The recent cryo-EM structure of the TCR CD3 complex afforded an opportunity to examine differences in the structure and dynamics in the TCR-only and TCR-pMHC systems by molecular dynamics.

Our simulations consisted of two membrane embedded TCR CD3 complexes with and without a second pMHC system. Two recent molecular dynamics studies of TCR-only systems based on the same cryo-EM structure, have recently been reported, allowing us to compare our TCR-only simulations and assess the generalizability of our observations (Prakaash et al., 2021) (Pandey et

al., 2021). Three main takeaways were consistent in all three molecular dynamics studies:

1) The pMHC-unbound TCR was highly dynamic, sampling a wide range of conformations
2) These conformations included states with even greater bending of the EC with respect to the membrane than in the initial cryo-EM structure
3) There was tight coupling between TCR and CD3 chains that were mediated by several regions in the TCR, including the FG loop

With these qualitative validations of our TCR-only simulations in hand, we next scrutinized the TCR-pMHC simulations, with the goal of identifying differences in the ITAM-containing CD3 chains. MD studies performed prior to release of the full TCR cryo-EM structure suggested that the TCR itself rigidified upon pMHC binding (Rangarajan et al., 2018). We observed that, indeed, fluctuations in the angle of the TCR headgroup with the plasma membrane were reduced in the TCR-pMHC system as compared to the TCR-only system, with a drop in the full-width at half maximum of ~10 degrees (Figure 4). However, while the TCR became less flexible, the CD3 co-receptors became more dynamic in the TCR-pMHC system. We rationalized these differences in terms of a "drawbridge" effect of the TCR and pMHC: when the TCR straightened to engage with the pMHC, it removed a brake on the CD3 chains, allowing them to diffuse around the TCR (Figure 5). The coupling between TCR and CD3s (mediated in part by the FG loop) was reduced significantly (Figure 3). This key observation nicely integrates the mechanosensor, allosteric relaxation and ITAM sequestration models into a coherent whole: Catch bonds hold the TCR-pMHC together, which decouples the TCR from the CD3 co-receptors (in particular CD3εγ), licensing CD3 co-receptor dynamics, ultimately leading to ITAM phosphorylation. This is a robust mechanism that is not dependent on specific details of the TCR CDRs. Rather, any TCR-pMHC interface of sufficient lifetime to allow CD3 diffusion underneath the drawbridge can lead to triggering.

# Acknowledgments

Simulations were performed using the Research Center for Computational Science, Okazaki, Japan (Projects: 20-IMS-C116, 21-IMS-C116 and 22-IMS-C116) and the TSUBAME3.0 supercomputer at Tokyo Institute of Technology. The authors wish to thank Misaki Ouchida for creating the illustration explaining the Dynamic Drawbridge model.

# Methods

Our interest in this project was to study a conventional TCR-MHC complex, but the extracellular part of the TCR electron densities of the De Dong structure have been fitted on the coordinates of an atypical natural killer TCR. For this reason, we fused the structure of the De Dong et al. (PDB ID 6jxr) (Dong et al., 2019) with the structure of a conventional TCR from Newell et al. (PDB ID 3qiu) (Newell et al., 2011). For the CD3 co-receptors and the transmembrane part of the TCR the structure of De Dong was used. The ITAM fragments were not present in the structure of De Dong and were modeled according to the murine sequence (see below). The structure by Newell et al served as the basis of MHC and of the extracellular parts of the TCR. It should be noted that the structure by De Dong is human, while the Newell structure and the modeled ITAM fragments are murine.

*MHC*

The structure from Newell et al lacks the MHC transmembrane helices, were modeled using HHpred (Zimmermann et al., 2018) and Pymol (Schrödinger, 2010). In order to obtain a realistic orientation of the two MHC transmembrane helices, a 10 µs coarse grained molecular dynamics simulation of the two helices embedded in a POPC bilayer composed out of 221 lipids was performed with the martini 3 force field (version v.3.0.4.26). The modeled atomistic helices were subsequently fitted on the simulated structures and connected to the soluble part of the MHC from Newell et al. using Modloop (Fiser and Sali, 2003). The epitope was restrained to the MHC using a number of harmonic potentials (Gromacs bondtype 6), see Table 4.

*TCR*

For the simulation a fusion of the structures of De Dong et al. and Newell et al. was created. From the structure of De Dong the CD3 co-receptors were taken, and the transmembrane segments of the α and β chains, which correspond to residue numbers 224-273 for the α chain and resid 264-308 for the β chain. The soluble segments of the TCRαβ chains were taken from the structure of Newell et al., for the α chain residues 2-199 and for the β chain residues 2-244,

please note that the residue numbering is according to the respective pdb files. The structures were fused using Pymol (Schrödinger, 2010) and Modloop (Fiser and Sali, 2003). One should note that the murine TCR has an extra disulfide bond between the TCR α and β subunits with respect to the human TCR, the cysteine bond between TCRα CYS156 and TCRβ CYS171 has no counterpart in the structure of De Dong.

Part of the missing and incomplete TCR and MHC residues were reconstructed using Spanner (Lis et al., 2011) and Pymol (Schrödinger, 2010), see Table 3. For a list of the residues that were included in the simulation, see Tables 1 & 2. ITAMs (immunoreceptor tyrosine-based activation motif) were modeled using Pymol. The TCR was coarse grained (see below), embedded in a membrane (see below) and a set of equilibration simulations was performed to equilibrate the ITAM chains.

*Positioning of TCR and MHC*

TCR and pMHC were carefully positioned on top of each other in preparatory 1.5 µs simulations. The TCR and MHC were embedded in opposing membrane slabs, which were separated by ~21 nm (GL1-GL1 bead distance) (Figure 1). A set of distance restraints based upon the Newell structure (PDB ID 3qiu) (Newell et al., 2011) was defined between TCR and pMHC (Table 6). During the 1.5 µs docking simulation a low force constant of 1 kJ $mol^{-1}$ $nm^{-2}$ was used to prevent any deformations. During the docking simulation the TCR and pMHC were slowly pulled together by the distance restraints resulting in a bound TCR-pMHC structure (Figure S1). In the production simulations a higher force constant of 200 kJ $mol^{-1}$ $nm^{-2}$ was used to keep the pMHC properly bound to the TCR. In order to allow solvent flow between the two membrane compartments, which in turns allows the bilayers to move, a pore was created in the bilayer containing the MHC. The pore was created using two cylinder shaped inverted flat bottom position restraints (function type 2, shape $g = 8$ in Gromacs). The first restraint, which was used to create the actual pore, acted on POPC beads with a force constant of 1000 kJ $mol^{-1}$ $nm^{-2}$ and a radius of 2 nm. The second restraint with a force constant of 2000 kJ $mol^{-1}$ $nm^{-2}$ and a radius of 4 nm acting on the MHC backbone beads was to make sure the MHC TM did not diffuse into the pore. Note that the preparatory simulations were performed for each of the one hundred TCR-pMHC simulations independently.

T cell receptor + CD3 co-receptors

| Protein name (Chain ID in PDB file (6jxr/3qiu)) | Residues in CG simulation | Section of ITAMs modelled | Residues in FG simulation |
|---|---|---|---|
| CD3$\zeta^{\varepsilon}$ (6jxr: A) | 22-164 | 57-164 | 22-56 |
| CD3$\zeta^{\gamma}$ (6jxr: B) | 24-164 | 56-164 | 24-55 |
| CD3δ (6jxr: D) | 22-173 | 130-173 | 22-129 |
| CD3$\varepsilon^{\delta}$ (6jxr: E) | 33-180 | 138-180[#]* | 33-155 |
| CD3$\varepsilon^{\gamma}$ (6jxr: F) | 33-180 | 138-180[#]* | 33-155 |
| CD3γ (6jxr: G) | 24-182 | 139-182 | 24-138 |
| TCRα (6jxr: M/3qiu: C)[$] | 2-249 | - | 2-249 |
| TCRβ (6jxr: N/3qiu: D)[$] | 2-293 | 290-293 | 2-289 |

MHC

| Protein name (Chain ID in PDB file (3qiu)) | Residues in CG simulation | Section of transmembrane helices modelled |
|---|---|---|
| MHCα (3qiu: A) | 3-230 | 182-230 |
| MHCβ (3qiu: B) | 3-231 | 187-231 |
| Epitope (3qiu: E) | 2-14 | - |

Table 1: Residues included in the simulation. In the ITAM column numbers between brackets refers to the uniprot numbering [#]The CD3ε ITAM sequence length differs between mouse and human, numbers refer to mouse sequence. *Erroneously residue 181-189 of the CD3ε chains (TCR E and TCR F) were omitted during modelling and not included in the simulation. [$]Numbering scheme of 3qiu is used, chain C for TCR α and chain D for TCRβ.

| | Residue numbering simulation | Residue Numbering 6jxr | Residue Numbering 3qiu | ITAMS modelled |
|---|---|---|---|---|
| TCRα | | | | |
| extra cellular section | 2-199 | - | 2-199 | |
| Transmembrane section | 200-249 | 224-273 | - | |
| ITAM section | - | - | - | - |
| TCRβ | | | | |
| extra cellular section | 2-244 | | 2-244 | |
| Transmembrane section | 245-288 | 264-308 | - | |
| ITAM section | 290-293 | - | - | 290-293 |

Table 2: Residues included in the simulation. In the ITAM column numbers between brackets refers to the uniprot numbering [#]The CD3ε ITAM sequence length differs between mouse and human, numbers refer to mouse sequence. *Erroneously residue 181-189 of the CD3$\varepsilon^{\delta}$ and CD3$\varepsilon^{\gamma}$ chains (TCR E and TCR F) were omitted during modelling and not included in the simulation. [$]Numbering scheme of 3qiu is used, chain C for TCRα and chain D for TCRβ.

| Protein | PDB ID | Chain | Residues |
|---|---|---|---|
| MHCβ | 3qiu | B | 105-113,134-135,165-170 |
| TCRα | 3qiu | C | 145-146, 175-179, 187-199 |
| TCRβ | 3qiu | D | 183-184, 219-220, 244 |
| CD3ζ | 6jxr | A | 57 *modelled with Pymol |
| CD3ε | 6jxr | F | 156 *modelled with Pymol |

Table 3: TCR and MHC residues which were reconstructed. Unless indicated, residues were reconstructed using Spanner (Lis et al., 2011).

| MHC chain | MHC residue number | MHC residue | MHC bead | Epitope residue number | Epitope residue | Epitope bead | Equilibrium distance (nm) | Force constant (kJ $mol^{-1}$ $nm^{-2}$) |
|---|---|---|---|---|---|---|---|---|
| A | 52 | ALA | BB | 2 | ALA | BB | 0.460 | 200 |
| B | 86 | PHE | SC2 | 5 | ILE | SC2 | 0.462 | 200 |
| A | 54 | PHE | SC2 | 5 | ILE | SC2 | 0.490 | 200 |
| B | 11 | CYS | SC1 | 10 | GLN | SC1 | 0.517 | 200 |
| B | 30 | TYR | SC4 | 11 | ALA | SC4 | 0.490 | 200 |
| A | 69 | ASN | SC1 | 12 | THR | SC1 | 0.507 | 200 |

Table 4: Harmonic potentials used to restrain the epitope in the MHC.

| Protein | Residue number | Protein | Residue number |
|---|---|---|---|
| $^{+}$CD3$\zeta^{\varepsilon}$ (chain A) | 32 | CD3$\zeta^{\gamma}$ (chain B) | 32 |
| CD3δ | 37 | CD3δ | 73 |
| CD3δ | 93 | CD3δ | 96 |
| CD3$\varepsilon^{\delta}$ (chain E) | 49 | CD3$\varepsilon^{\delta}$ (chain E) | 98 |
| CD3$\varepsilon^{\delta}$ (chain E) | 119 | CD3$\varepsilon^{\delta}$ (chain E) | 122 |
| CD3$\varepsilon^{\gamma}$ (chain F) | 49 | CD3$\varepsilon^{\gamma}$ (chain F) | 98 |
| CD3$\varepsilon^{\gamma}$ (chain F) | 119 | CD3$\varepsilon^{\gamma}$ (chain F) | 122 |
| CD3γ | 46 | CD3γ | 87 |
| CD3γ | 104 | CD3γ | 107 |
| TCRα | 22 | TCRα | 86 |
| TCRα | 131 | TCRα | 181 |
| $^{+}$TCRα | 156 | TCRβ | 171 |
| $^{+}$TCRα | 203 | TCRβ | 245 |
| TCRβ | 23 | TCRβ | 92 |
| TCRβ | 69 | TCRβ | 75 |
| TCRβ | 145 | TCRβ | 210 |
| MHCα | 105 | MHCα | 163 |
| MHCβ | 15 | MHCβ | 79 |
| MHCβ | 117 | MHCβ | 173 |

Table 5: Disulfide bonds present in the simulation. $^{+}$Inter-chain disulfide bond are modeled by a harmonic potential.

| MHC chain | MHC residue number | MHC residue | MHC bead | TCR chain | TCR residue number | TCR residue | TCR bead | $r_0$ (nm) | $r_1$ (nm) | $r_2$ (nm) | Force constant (kJ mol$^{-1}$ nm$^{-2}$) |
|---|---|---|---|---|---|---|---|---|---|---|---|
| MHCβ | 69 | GLU | BB | TCRα | 49 | ALA | BB | 0.593 | 0.693 | 3.093 | 200 |
| MHCβ | 77 | THR | BB | TCRα | 29 | ARG | BB | 0.482 | 0.582 | 3.682 | 200 |
| MHCβ | 84 | GLU | BB | TCRα | 65 | LYS | BB | 1.102 | 1.202 | 4.302 | 200 |
| MHCα | 57 | GLN | BB | TCRβ | 57 | GLN | BB | 0.788 | 0.888 | 3.988 | 200 |
| MHCα | 61 | ALA | BB | TCRβ | 33 | PHE | BB | 1.211 | 1.311 | 4.411 | 200 |
| MHCα | 75 | GLU | BB | TCRβ | 53 | GLU | BB | 1.800 | 1.900 | 5.000 | 200 |
| MHCε | 6 | ALA | BB | TCRα | 92 | SER | BB | 0.320 | 0.480 | 3.520 | 200 |
| MHCε | 11 | ALA | BB | TCRβ | 98 | ASN | BB | 0.429 | 0.529 | 3.629 | 200 |
| MHCα | 61 | ALA | BB | TCRβ | 55 | LEU | BB | 0.365 | 0.465 | 3.565 | 200 |
| MHCα | 64 | ALA | BB | TCRβ | 55 | LEU | BB | 0.560 | 0.660 | 3.760 | 200 |
| MHCα | 57 | GLN | BB | TCRβ | 55 | LEU | BB | 0.739 | 0.839 | 3.939 | 200 |
| MHCα | 64 | ALA | BB | TCRβ | 53 | GLU | BB | 0.649 | 0.749 | 3.849 | 200 |
| MHCα | 57 | GLN | BB | TCRβ | 53 | GLU | BB | 1.327 | 1.447 | 4.547 | 200 |
| MHCα | 61 | ALA | BB | TCRβ | 57 | GLN | BB | 0.917 | 1.067 | 4.167 | 200 |
| MHCα | 64 | ALA | BB | TCRβ | 57 | GLN | BB | 1.231 | 1.331 | 4.431 | 200 |
| MHCα | 57 | GLN | BB | TCRβ | 33 | PHE | BB | 1.421 | 1.521 | 4.621 | 200 |
| MHCα | 64 | ALA | BB | TCRβ | 33 | PHE | BB | 1.441 | 1.541 | 4.641 | 200 |
| MHCα | 64 | ALA | BB | TCRβ | 49 | PHE | BB | 0.899 | 0.999 | 4.099 | 200 |
| MHCα | 65 | VAL | BB | TCRβ | 49 | PHE | BB | 0.916 | 1.016 | 5.116 | 200 |
| MHCα | 61 | ALA | BB | TCRβ | 49 | PHE | BB | 0.843 | 0.943 | 5.043 | 200 |
| MHCβ | 73 | ALA | BB | TCRα | 49 | ALA | BB | 0.528 | 0.728 | 1.828 | 200 |
| MHCβ | 66 | GLU | BB | TCRα | 49 | ALA | BB | 0.706 | 0.806 | 2.006 | 200 |
| MHCβ | 73 | ALA | BB | TCRα | 29 | ARG | BB | 0.664 | 0.764 | 1.964 | 200 |
| MHCβ | 74 | GLU | BB | TCRα | 29 | ARG | BB | 0.625 | 0.725 | 3.825 | 200 |
| MHCβ | 76 | ASP | BB | TCRα | 65 | LYS | BB | 0.643 | 0.743 | 3.602 | 200 |
| MHCβ | 73 | ALA | BB | TCRα | 65 | LYS | BB | 0.930 | 1.030 | 4.130 | 200 |

Table 6: List of distance restraints between the TCR and the pMHC. Note that during the docking simulations the force constant was set to 1 kJ mol$^{-1}$ nm$^{-2}$. A piecewise linear/harmonic restraint was used (bond type 10 in Gromacs) to keep the TCR and the pMHC together. The potential is quadratic for $r_{ij} < r_0$, 0 for $r_0 \leq r_{ij} < r_1$, quadratic for $r_1 \leq r_{ij} < r_2$ and linear for $r_2 \leq r_{ij}$.

*Coarse graining and run parameters*

Simulations were performed with the Martini 3 force field, version v.3.0.4.26 (Souza et al., 2021) in combination with a Gō-like model (Thallmair et al., 2019) (Poma et al., 2017). Coarse grained topologies were created using Martinize2 (Kroon, 2020). Simulations were performed with Gromacs, versions 2018-2022 (Abraham et al., 2015) with a 20 fs timestep and the 'New-RF' parameter set for the Martini force field (de Jong et al., 2016) with the modification that the Berendsen barostat was used. Temperature was kept at 310 K using the V-rescale thermostat (Bussi et al., 2007) using a coupling constant of $\tau_t = 1$ ps. Pressure was semiisotropically coupled to an external bath of p = 1 bar with a coupling constant of $\tau_p = 4$ ps and a compressibility of $\chi = 3 \times 10^{-4}$ bar$^{-1}$ using the Berendsen barostat (Berendsen et al., 1984).

*Simulation systems*

The protein systems were embedded in POPC bilayers using the Insane script(Wassenaar et al., 2015). The TCR was embedded in a POPC bilayer of 1279 lipids (651 lipids in the extracellular leaflet and 628 lipids in the intracellular leaflet). The pMHC was embedded in a POPC bilayer of 1278 lipids (640 lipids in the extracellular leaflet and 638 lipids in the intracellular leaflet). The TCR only system was solvated in 90282 water beads (representing 361128 atomistic waters) and 1018 $Na^+Cl^-$ beads were added (around 154 mM) and an additional 6 $Cl^-$ ions to neutralize the system. The TCR-pMHC system was solvated in 95973 water beads (representing 383892 atomistic waters) and 1079 $Na^+Cl^-$ beads were added (around 154 mM) and an additional 12 $Na^+$ ions to neutralize the system. One hundred independent 10 µs production simulations were performed for both the TCR-only and TCR-pMHC systems. Note that each TCR-pMHC production run was preceded by a 1.5 µs preparatory simulation in which the TCR was slowly docked to the pMHC.

*Analysis*

The first 1 µs of each production simulation was discarded as equilibration, and the remaining (9 µs) trajectories were analyzed every 10 ns. The angle between the TCRβ EC and TM was calculated for simulation systems between the backbone beads of asparagine 97 serine 249 and valine 281 of the TCR β chain and for the cryo-EM structure between the Cα atoms of arginine 114, serine 268 and valine 300. Note that serine 249/268 and valine 281/300 are the corresponding residues in the simulation systems and cryo-EM structure, arginine 114 was chosen for its proximity to asparagine when superimposing simulated structure and the cryo-EM structure. Iso-occupancy maps were calculated using the Volmap tool in VMD. Grid spacing was set to 2 Å and counting of grid occupancy was performed after fitting the trajectories on the backbone beads of the TCR chains. Contacts between the TCR and CD3 co-receptor chains were calculated with inhouse python scripts making use of the MDAnalysis library (Gowers et al., 2016; Michaud-Agrawal et al., 2011). Beads were considered in contact when their distance was < 6 Å, and residue contacts were calculated by summing all bead contacts. The following residues were considered to be part of the constant, variable, transmembrane and cytosolic domains for the TCR chains: TCRα variable: 1-106, constant: 107-198, transmembrane: 199-246, cytosolic: 247-249. TCRβ variable: 1-117, constant: 118-245, transmembrane: 246-285, cytosolic: 286-293. Trajectories were viewed using VMD and ChimeraX and pictures were rendered with ChimeraX (Humphrey et al., 1996; Goddard et al., 2018; Pettersen et al., 2021).

# Bibliography


Abraham, Mark James, et al. (2015), 'GROMACS: High performance molecular simulations through multi-level parallelism from laptops to supercomputers', *SoftwareX*, 1 19-25.

Aivazian, D and LJ Stern (2000), 'Phosphorylation of T cell receptor zeta is regulated by a lipid dependent folding transition.', *Nat Struct Biol*, 7 (11), 1023-26.

Al-Aghbar, MA, et al. (2022), 'The interplay between membrane topology and mechanical forces in regulating T cell receptor activity.', *Commun Biol*, 5 (1), 40.

Alba, J, et al. (2020), 'Molecular Dynamics Simulations Reveal Canonical Conformations in Different pMHC/TCR Interactions.', *Cells*, 9 (4), E942.

Beddoe, Travis, et al. (2009), 'Antigen ligation triggers a conformational change within the constant domain of the αβ T cell receptor', *Immunity*, 30 (6), 777-88.

Bello, Martiniano and Jose Correa-Basurto (2016), 'Energetic and flexibility properties captured by long molecular dynamics simulations of a membrane-embedded pMHCII–TCR complex', *Molecular BioSystems*, 12 (4), 1350-66.

Berendsen, HJC, et al. (1984), 'Molecular dynamics with coupling to an external bath', *The Journal of Chemical Physics*, 81 (8), 3684-90.

Brameshuber, M, et al. (2018), 'Monomeric TCRs drive T cell antigen recognition.', *Nat Immunol*, 19 (5), 487-96.

Brazin, Kristine N, et al. (2018), 'The T Cell Antigen Receptor α Transmembrane Domain Coordinates Triggering through Regulation of Bilayer Immersion and CD3 Subunit Associations', *Immunity*, 49 (5), 829-841.e6.

Bussi, Giovanni, Davide Donadio, and Michele Parrinello (2007), 'Canonical sampling through velocity rescaling', *The Journal of Chemical Physics*, 126 (1), 014101.

Cai, Haogang, et al. (2018), 'Full control of ligand positioning reveals spatial thresholds for T cell receptor triggering', *Nature Nanotechnology*, 1-11.

Das, DK, et al. (2015), 'Force-dependent transition in the T-cell receptor β-subunit allosterically regulates peptide discrimination and pMHC bond lifetime.', *Proc Natl Acad Sci U S A*, 112 (5), 1517-22.

Davis, SJ and PA van der Merwe (2006), 'The kinetic-segregation model: TCR triggering and beyond.', *Nat Immunol*, 7 (8), 803-9.

de Jong, Djurre H, et al. (2016), 'Martini straight: Boosting performance using a shorter cutoff and GPUs', *Computer Physics Communications*, 199 1-7.

Dong, De, et al. (2019), 'Structural basis of assembly of the human T cell receptor–CD3 complex', *Nature*, 1-21.

Feng, Y., E. L. Reinherz, and M. J. Lang (2018), 'alphabeta T Cell Receptor Mechanosensing Forces out Serial Engagement', *Trends Immunol*, 39 (8), 596-609.

Fiser, András and Andrej Sali (2003), 'ModLoop: automated modeling of loops in protein structures', *Bioinformatics*, 19 (18), 2500-1.

Goddard, TD, et al. (2018), 'UCSF ChimeraX: Meeting modern challenges in visualization and analysis.', *Protein Sci*, 27 (1), 14-25.

Gowers, Richard J, et al. (2016), 'MDAnalysis: A Python package for the rapid analysis of molecular dynamics simulations', *Proceedings of the 15th Python in Science Conference*, 102-9.
Humphrey, William, Andrew Dalke, and Klaus Schulten (1996), 'VMD: Visual molecular dynamics', *Journal of Molecular Graphics*, 14 (1), 33-38.
Hwang, W, et al. (2020), 'The αβTCR mechanosensor exploits dynamic ectodomain allostery to optimize its ligand recognition site.', *Proc Natl Acad Sci U S A*, 117 (35), 21336-45.
Kim, S. T., et al. (2009), 'The alphabeta T cell receptor is an anisotropic mechanosensor', *J Biol Chem*, 284 (45), 31028-37.
Kroon, PC (2020), 'Automate, aggregate, assemble', (Dissertation, University of Groningen).
Lanz, AL, et al. (2021), 'Allosteric activation of T cell antigen receptor signaling by quaternary structure relaxation.', *Cell Rep*, 36 (2), 109375.
Lis, Mieszko, et al. (2011), 'Bridging the gap between single-template and fragment based protein structure modeling using Spanner', *Immunome Research*, 7 (1), 1.
Lo, Wan-Lin, et al. (2019), 'Slow phosphorylation of a tyrosine residue in LAT optimizes T cell ligand discrimination', *Nature Publishing Group*, 1-19.
Mariuzza, Roy A., Pragati Agnihotri, and John Orban (2020), 'The structural basis of T-cell receptor (TCR) activation: An enduring enigma', *Journal of Biological Chemistry*, 295 (4), 914-25.
Michaud-Agrawal, Naveen, et al. (2011), 'MDAnalysis: a toolkit for the analysis of molecular dynamics simulations.', *Journal of Computational Chemistry*, 32 (10), 2319-27.
Natarajan, Kannan, et al. (2017), 'An allosteric site in the T-cell receptor Cβ domain plays a critical signalling role', *Nature communications*, 8 (1), 1-14.
Newell, Evan W, et al. (2011), 'Structural basis of specificity and cross-reactivity in T cell receptors specific for cytochrome c-I-Ek', *Journal of immunology (Baltimore, Md.: 1950)*, 186 (10), 5823-32.
Nika, K, et al. (2010), 'Constitutively active Lck kinase in T cells drives antigen receptor signal transduction.', *Immunity*, 32 (6), 766-77.
Pandey, Prithvi R, et al. (2021), 'Structural variability and concerted motions of the T cell receptor-CD3 complex', *eLife*, 10
Pettersen, EF, et al. (2021), 'UCSF ChimeraX: Structure visualization for researchers, educators, and developers.', *Protein Sci*, 30 (1), 70-82.
Poma, Adolfo B, Marek Cieplak, and Panagiotis E Theodorakis (2017), 'Combining the MARTINI and Structure-Based Coarse-Grained Approaches for the Molecular Dynamics Studies of Conformational Transitions in Proteins', *Journal of Chemical Theory and Computation*, 13 (3), 1366-74.
Prakaash, D, et al. (2021), 'Multi-scale simulations of the T cell receptor reveal its lipid interactions, dynamics and the arrangement of its cytoplasmic region.', *PLoS Comput Biol*, 17 (7), e1009232.
Rangarajan, Sneha, et al. (2018), 'Peptide-MHC (pMHC) binding to a human antiviral T cell receptor induces long-range allosteric communication between pMHC- and CD3-binding sites.', *The Journal of biological chemistry*, 293 (41), 15991-6005.
Saito, Takashi and Tadashi Yokosuka (2006), 'Immunological synapse and microclusters: the site for recognition and activation of T cells', *Current Opinion in Immunology*, 18 (3), 305-13.
Schrödinger, LLC (2010), 'The PyMOL Molecular Graphics System, Version 1.7.0.0.',

Sokurenko, EV, V Vogel, and WE Thomas (2008), 'Catch-bond mechanism of force-enhanced adhesion: counterintuitive, elusive, but. widespread', *Cell Host Microbe*, 4 314-23.

Souza, PCT, et al. (2021), 'Martini 3: a general purpose force field for coarse-grained molecular dynamics.', *Nat Methods*, 1-7.

Thallmair, Sebastian, Petteri A Vainikka, and Siewert J Marrink (2019), 'Lipid Fingerprints and Cofactor Dynamics of Light-Harvesting Complex II in Different Membranes', *Biophysical journal*, 116 (8), 1446-55.

van der Merwe, PA and O Dushek (2011), 'Mechanisms for T cell receptor triggering.', *Nat Rev Immunol*, 11 (1), 47-55.

Wan, S, DR Flower, and PV Coveney (2008), 'Toward an atomistic understanding of the immune synapse: large-scale molecular dynamics simulation of a membrane-embedded TCR-pMHC-CD4 complex.', *Mol Immunol*, 45 (5), 1221-30.

Wassenaar, Tsjerk A, et al. (2015), 'Computational Lipidomics with insane: A Versatile Tool for Generating Custom Membranes for Molecular Simulations.', *Journal of Chemical Theory and Computation*, 11 (5), 2144-55.

Xu, C., et al. (2008), 'Regulation of T cell receptor activation by dynamic membrane binding of the CD3epsilon cytoplasmic tyrosine-based motif', *Cell*, 135 (4), 702-13.

Zhu, Cheng, et al. (2019), 'Mechanosensing through immunoreceptors', *Nature Publishing Group*, 1-10.

Zimmermann, Lukas, et al. (2018), 'A completely reimplemented MPI bioinformatics toolkit with a new HHpred server at its core', *Journal of molecular biology*, 430 (15), 2237-43.